JES Focus Issue on Redox Flow Batteries—Reversible Fuel Cells

# High Surface Area Carbon Electrodes for Bromine Reactions in $H_2$-$Br_2$ Fuel Cells

**Venkata Yarlagadda,[a,*] Guangyu Lin,[b,**] Pau Ying Chong,[b] and Trung Van Nguyen[a,***,z]**

[a]*Department of Chemical and Petroleum Engineering, The University of Kansas, Lawrence, Kansas 66045, USA*
[b]*TVN Systems, Inc., Lawrence, Kansas 66046, USA*

In a hydrogen-bromine ($H_2$-$Br_2$) fuel cell, the $Br_2$ reactions don't require precious metal catalysts, hence porous carbon gas diffusion media (GDM) are widely used as electrodes. However, the specific surface areas of the commercial carbon gas diffusion electrodes (GDEs) are quite low and need to be enhanced. In order to improve the active surface area of carbon GDEs, a study was conducted to grow multi-walled carbon nanotubes (MWCNTs) directly on the carbon electrode fiber surface. Both constant and pulse current electrodeposition techniques were used to deposit Co nanoparticles to catalyze the MWCNT growth. The MWCNTs were grown in the presence of a mixture of acetylene, argon, and hydrogen gases using the chemical vapor deposition process. Based on the results obtained from SEM, TEM, and EDX analysis, MWCNT growth following the tip model was confirmed. The results from the multi-step chronoamperometry study have shown that the synthesized carbon GDEs with MWCNTs have 7 to 50 times higher active surface area than that of a plain GDE. The performance of a single layer of the best MWCNT GDE measured in a $H_2$-$Br_2$ fuel cell was found to be equal or slightly higher compared to that obtained using a three-layer plain carbon electrode.


Manuscript submitted August 3, 2015; revised manuscript received September 21, 2015. Published October 30, 2015. This was Paper 545 presented at the Orlando, Florida, Meeting of the Society, May 11–15, 2014. *This paper is part of the JES Focus Issue on Redox Flow Batteries–Reversible Fuel Cells.*

Electrical energy storage is required to address the increasing use of intermittent energy sources. The regenerative hydrogen-bromine ($H_2$-$Br_2$) fuel cell was identified as a promising candidate for large scale electrical energy storage due to the rapid kinetics of the $H_2$ and $Br_2$ reactions translating to its higher energy conversion efficiency and power density capability.[1–8] Moreover, the abundance of active materials used in this system is an added advantage. The electrochemical reactions associated with the $H_2$-$Br_2$ fuel cell system are shown below.

$$H_2 \text{ electrode: } H_2 \underset{\text{charge}}{\overset{\text{discharge}}{\rightleftharpoons}} 2H^+ + 2e^- \quad E^o = 0\,V$$

$$Br_2 \text{ electrode: } Br_2 + 2e^- \underset{\text{charge}}{\overset{\text{discharge}}{\rightleftharpoons}} 2Br^- \quad E^o = 1.09\,V$$

$$\text{Overall: } H_2 + Br_2 \underset{\text{charge}}{\overset{\text{discharge}}{\rightleftharpoons}} 2HBr \quad E^o = 1.09\,V$$

The bromine electrode in the $H_2$-$Br_2$ fuel cell can be replaced by alternative materials such as vanadium, cesium, chromium or iron. However, the $H_2$-$Br_2$ system is more attractive than the hydrogen-vanadium[9] because its active material (HBr) is inexpensive, its electrode reaction kinetics are much faster, and it has much higher energy density (higher HBr/$Br_2$ concentrations and no supporting electrolyte required because HBr serves as both the reactive material and electrolyte). On the other hand, cesium is a rare earth element and is very expensive ($10/gram or $300/ounce) making it unsuitable for large scale energy storage. Also, the cesium, chromium, and iron systems have not been explored with a negative hydrogen electrode.

While the $H_2$ reactions currently require the use of precious metal catalysts like platinum, the bromine reactions don't since reasonable exchange current densities can be obtained with carbon materials.[6] Even though the exchange current density of $Br_2$ reactions on platinum (Pt) is two orders of magnitude higher than that on carbon materials, the corrosivity and toxicity of hydrobromic acid (HBr) and $Br_2$ species make it impractical to use any noble metal catalysts in the $Br_2$ electrode.[10] One way to solve the lower exchange current density of $Br_2$ reactions on plain carbon electrodes is to increase the mass specific active surface area of the electrode. Typically, carbon gas diffusion electrodes (GDEs) with high porosity are the optimal choice due to the presence of corrosive aqueous reactants (hydrobromic acid and bromine). The high porosity allows more active materials to be stored near where they are needed and facilitates easy fluid flow to access most of the active surface area of the carbon electrode. Hence, it is important that the morphological properties (porosity and tortuosity) of the carbon electrode remain undisturbed while improving the active surface area.

The specific active surface area (intrinsic property) of commercially available untreated carbon GDEs is quite low (0.65 $m^2/g$ compared to 100 $m^2/g$ of Pt/C electrodes).[11] One of the common approaches reported in the literature to improve the active surface area of a $Br_2$ electrode was to employ multiple layers of carbon GDEs.[6,8] A major disadvantage of this approach is that the thickness (bulk property) of the $Br_2$ electrode increases with the number of carbon GDE layers used resulting in longer ionic, electronic, and molecular diffusion pathways. This could lead to mass transport-limited performance at higher current densities.[12] Several previous studies have investigated high surface area carbon materials such as carbon nanotubes, graphene-based nanoplatelets, and activated carbon powders for battery and electrochemical capacitor applications.[13,14] However, these high surface area carbon materials are normally blended with a polymeric binder of some kind in order to fabricate solid carbon electrodes for fuel cell applications. The resulting electrodes are usually dense and have low porosity and high tortuosity, which are undesirable especially if the reactants are in an aqueous phase. The other approach to enhance the active surface area of existing carbon GDE is to coat them with an ink or suspension prepared from high surface area carbon materials. A major limitation associated with this approach is that the high surface area carbon materials are attached to the carbon electrode fiber surface by means of weak Van Der Waals forces and might be removed at high liquid reactant flow rates or by physical changes in the electrodes during operation. In conclusion, durable high surface area carbon materials with high porosity and tortuosity that can withstand high liquid flow rates are required.

Several studies in the literature have reported different approaches to enhance the active surface area of an existing carbon GDE

*Electrochemical Society Student Member.
**Electrochemical Society Active Member.
***Electrochemical Society Fellow.
[z]E-mail: cptvn@ku.edu

without affecting its morphological properties. Etching processes such as chemical and plasma (argon or oxygen ion) etching are widely used to improve the active surface area of existing porous carbon electrodes.[15,16] The etching processes create roughness and introduce functional groups on the carbon electrode fiber surface, which in turn increases the active surface area of the electrode. Some limitations associated with these etching techniques involve the expensive nature of plasma etching and chemical impurities that might be incorporated if the chemically etched carbon electrode is not cleaned properly. A recent study by Mayrhuber et al. used a laser perforation technique to improve the transport characteristics of some commercial porous carbon electrodes by creating holes in their microstructure despite losing some active surface area.[17] However, the laser perforation technique is quite expensive and only improves the cell performance in the transport controlled regime. A few approaches reported in the literature have tried to improve the surface area of existing porous carbon electrodes by connecting the carbon nanotubes (CNTs) to the carbon electrode fiber surface by means of a covalent bond.[18–21] The covalent bond between CNTs and the carbon electrode fiber surface is quite strong and can withstand high liquid reactant flow rates.

There are several ways to synthesize CNTs either directly on substrates such as silicon, alumina, and quartz or on the porous carbon electrode fiber surface. Because of their attractive properties, such as high electronic conductivity, large specific surface area, and excellent chemical stability, CNTs are often used as an electrode material for electrochemical energy storage devices. The CNTs are classified into two types; single-walled and multi-walled carbon nanotubes (SWCNTs and MWCNTs). For the fuel cell and battery applications, MWCNTs are more preferable due to their high electrical conductivity and mechanical durability compared to that of SWCNTs. Also, the outer graphene shells of MWCNTs protect the inner ones from degradation thus prolonging their lifetime. Carbon arc-discharge, laser ablation, and chemical vapor deposition are some of the techniques used to synthesize CNTs.[22–24] Ijima et al. discovered carbon nanotubes in 1991 using arc-discharge technique,[25] and since then chemical vapor deposition (CVD) has been widely used to synthesize both single and multi-walled carbon nanotubes. The CVD process requires less energy compared to arc-discharge and laser ablation techniques making it a suitable option for large scale synthesis widely used to synthesize CNTs. The CNT-based carbon electrodes were also proven to be excellent candidates for supercapacitors due to their high specific surface areas.[20]

In order to synthesize CNTs directly on the carbon electrode fiber surface via CVD process, nanocatalyst seeds are required to catalyze the CNT growth. The transition metals (iron, cobalt, and nickel) are known to be active catalysts for CNT synthesis.[26] The catalyst seeds are created on the carbon electrode fiber surface using techniques such as electron beam evaporation, electrodeposition, and solution deposition.[18–21] Out of the techniques listed above, electrodeposition is more cost effective and hence a suitable option for depositing the catalyst nanoparticles on the carbon electrode fiber surface. After depositing the catalyst nanoparticles, CNTs are usually synthesized in the presence of a hydrocarbon gas (carbon source) between 700°C and 1000°C. Some of the recent studies have used the spray pyrolysis approach to synthesize CNTs by using a xylene (carbon source)/ferrocene (catalyst source) precursor solution.[27,28] However, the spray pyrolysis process is a bit involved since a separate chamber is required to vaporize the xylene/ferrocene precursor solution before introducing it into the reactor furnace. The incomplete vaporization of the precursor solution directly affects the catalyst deposition.

In this paper, experimental approaches concerning electrodeposition of Co nanoparticles and MWCNT growth using CVD process on a carbon GDE (SGL 10AA GDE from Sigracet) are discussed and the results are presented. The results involve electrochemical active surface area measurements of the synthesized MWCNT-based electrodes in a three-electrode arrangement followed by the performance comparison between MWCNT-based carbon electrode and plain porous carbon GDE in a $H_2$-$Br_2$ fuel cell.

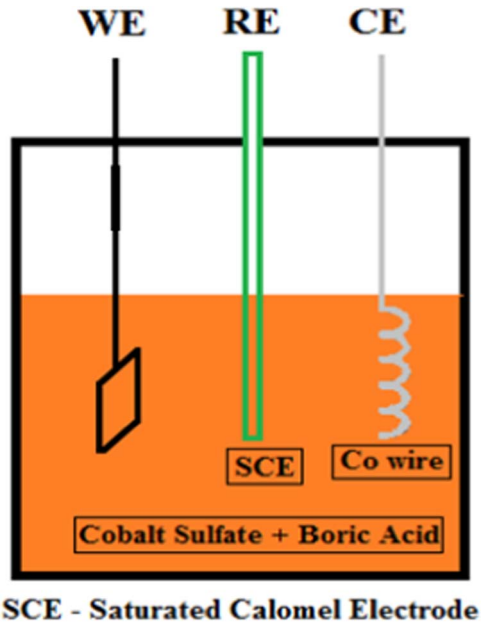


**Figure 1.** Experimental fixture used in the electrodeposition experiment.

## Experimental

*Synthesis of MWCNT-based carbon electrodes.*— The synthesis of MWCNT-based electrodes involves two major steps: 1) electrodeposition of nano catalyst particles and 2) growth of CNTs on carbon fiber surface. The first step involves creating active metal catalyst sites on the electrode fiber matrix for the hydrocarbon source to react and form nanotube structures. Since transition metals are known to be active catalysts for carbon nanotube synthesis, cobalt (Co) was chosen as the catalyst for this study. The Co nanoparticles were deposited on the SGL 10AA carbon electrode fiber surface by both constant and pulse current electrodeposition techniques in a solution containing cobalt sulfate ($CoSO_4$) and boric acid ($H_3BO_3$). The role of $H_3BO_3$ in the precursor solution was to avoid the formation of an insoluble hydroxide phase at the carbon electrode/electrolyte interface by maintaining the pH of the electrolyte solution in the acidic range (between 4.4 and 4.6).[29] The electrolyte solution is a mixture of 0.02 M $CoSO_4$ and 0.33 M $H_3BO_3$.

A three-electrode arrangement was used to implement constant and pulse current electrodeposition techniques. The experimental setup (shown in Figure 1) consisted of a SGL 10 AA carbon electrode and a saturated calomel (SCE) reference electrode. A coiled cobalt wire was used as the counter electrode. The Co catalyst was deposited by applying a cathodic current to the working electrode. The current collection was done using stainless steel alligator clips. Prior to the electrodeposition experiment, carbon electrodes were boiled in deionized (DI) water for 1 hour to make them hydrophilic. Also, a case study was done to study the effect of soaking the carbon electrodes in an electrolyte solution (mixture of cobalt sulfate and boric acid) for 24 hours after boiling them in DI water and before conducting the electrodeposition experiment. The concentration of the precursor solution that the carbon electrodes were soaked in was the same as that of the solution used in the electrodeposition step. A total of 5 carbon electrode samples were synthesized using constant and pulse current electrodeposition. The first two samples were synthesized using constant current electrodeposition (sample 1: $-0.1$ mA/cm$^2$ for 1000s, and sample 2: $-0.1$ mA/cm$^2$ for 2000s). The geometric area of sample 1 and sample 2 was 9 cm$^2$. The rest of the samples were synthesized using pulse current electrodeposition (sample 3: $-3.75$ mA/cm$^2$ applied with a single pulse of 1s, sample 4: $-5$ mA/cm$^2$ applied with two pulses each with a 0.1s duration, and sample 5: $-2.5$ mA/cm$^2$ applied with a single pulse of 1s). The geometric area of sample 3, sample 4, and sample 5 was 4 cm$^2$. Finally, Scanning Electron

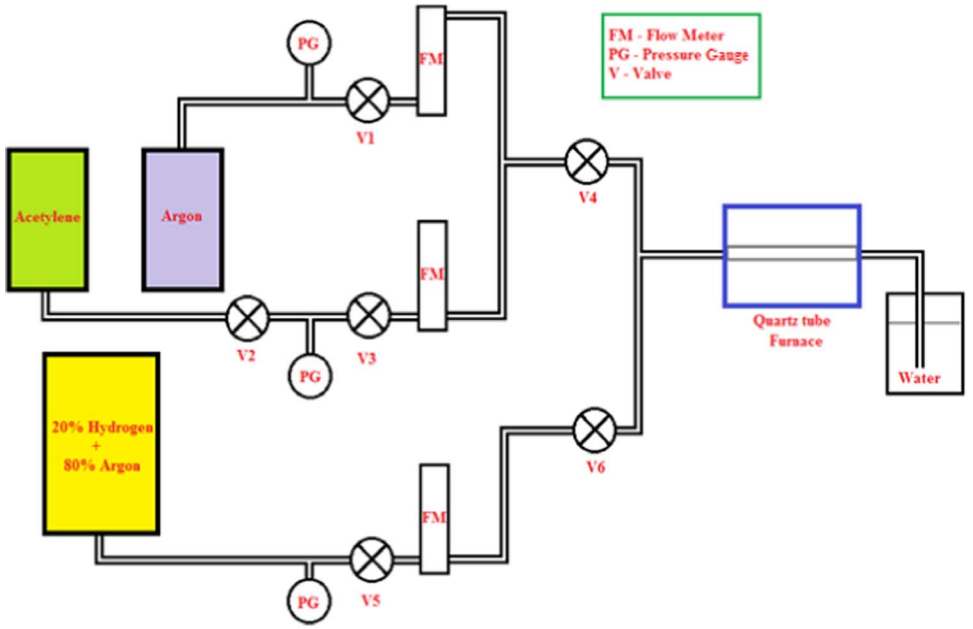


**Figure 2.** Experimental set-up used to perform CVD for MWCNT synthesis.

Microscopy (SEM) analysis was used to confirm the electrodeposition of Co nanoparticles on the carbon electrode fiber surface.

The second step for synthesizing carbon nanotube based electrodes involves growing MWCNTs in the presence of an acetylene ($C_2H_2$), argon (Ar), and hydrogen ($H_2$) gas mixture at high temperatures. In the gas mixture, $C_2H_2$ was used as the carbon source, Ar was used to prevent the carbon paper from combusting and to dilute the acetylene gas and $H_2$ was used to prevent soot formation resulting from carbon pyrolysis. The experimental set-up used for this process is shown in Figure 2. Initially, the catalyst coated carbon electrodes were placed in the quartz tube furnace (MTI corporation, model: OTF-1200X-S) and heated to 550°C at a ramp rate of 3°C/min starting from 25°C or room temperature in the presence of a mixture of 20% $H_2$ and 80% Ar gas (flow rate: 80 cc/min). The carbon electrodes were allowed to stay at 550°C for 45 minutes to reduce any cobalt oxide present on the surface of the Co nanoparticles. Next, the carbon electrodes were heated to 700°C (reaction temperature) from 550°C at a 4°C/min ramp rate. At 700°C, a mixture of $C_2H_2$ (flow rate: 10 cc/min) and Ar (flow rate: 60 cc/min) gas was introduced to initiate the MWCNT growth. The carbon electrodes were allowed to stay at 700°C for 30 minutes to grow MWCNTs. Finally, the $C_2H_2$ and $H_2$ sources were shut off and the carbon electrodes were cooled in the presence of Ar gas. In addition to the catalyst coated carbon electrodes, a plain SGL 10AA electrode was heat-treated in the quartz tube reactor in the presence of hydrogen and argon gas using the operating conditions described above. This was done to determine whether the active surface of the carbon GDM could be altered by the high temperature treatment condition used in the MWCNT growth process.

The synthesized carbon electrodes were sonicated in de-ionized (DI) water for 30 minutes to get rid of any amorphous carbon and other impurities present in the carbon electrode and subsequently soaked in 1 M nitric acid ($HNO_3$) overnight to etch away the exposed Co metal nanoparticles. The electrodes were washed in DI water after the acid treatment and subsequent SEM analysis was done to confirm the MWCNT growth. Also, Transmission Electron Microscopy (TEM) and Energy Dispersive X-ray Spectroscopy (EDX) were used to determine the growth mechanism of MWCNTs on the carbon electrode fiber surface.

*Surface area enhancement measurements.*— The heat-treated and MWCNT-based carbon electrodes were electrochemically analyzed using the linearized Butler-Volmer approach to determine the increase in their specific active areas compared to that of a plain carbon electrode.[7] The Butler-Volmer equation, when the overpotentials are below ±25 mV, can be linearized as follows:

$$i \cong ai_o\left[(\alpha_a + \alpha_c)\left(\frac{F}{RT}\eta\right)\right] \cong \frac{ai_oFn}{RT}\eta \qquad [1]$$

where $i$ is the electrode current density (in A/g), $a$ is the active surface area (in $cm^2/g$), $i_o$ is the exchange current density ($A/cm^2$), $F$ is the Faraday constant, $R$ is the gas constant (in J/mol.K), $T$ is the temperature (in K), $\eta$ is the overpotential (in V), $n$ is the number of electrons, and $\alpha_a$ and $\alpha_c$ are the anodic and cathodic transfer coefficients.

A three-electrode arrangement was used to perform the electrochemical analysis in a solution of 1 M HBr and 0.1 M $Br_2$. The carbon electrode (plain, heat-treated, and MWCNT-based) and a saturated calomel electrode were used as the working electrode (WE) and reference electrode (RE) respectively. A platinum foil was used as the counter electrode. Multi-step chronoamperometry was conducted with the applied overpotentials ranging between −12 and +12 mV. The solution resistance between the working and reference electrodes was measured using Electrochemical Impedance Spectroscopy (Gamry EIS 300, Amplitude: 5 mV and Frequency range: 0.1 Hz to 100 kHz). The linearized Butler-Volmer equation approach was used to calculate the product of the specific active area ($a$) and the exchange current density ($i_o$) of plain SGL 10AA, heat-treated SGL 10AA and MWCNT-based carbon electrodes (Samples 1 to 5). The factor $ai_o$ for the heat-treated and MWCNT-based carbon electrodes was normalized to that of a plain SGL 10AA carbon electrode to calculate the active area enhancement factors as follows.

$$Enhancement\ factor = \frac{(ai_o)_{MWCNT\ or\ heat-treated\ electrode}}{(ai_o)_{Plain}} \qquad [2]$$

*Fuel cell measurements.*— The performance of a plain 0.1245 cm thick SGL 10AA (3 pieces of SGL 10AA stacked together) and a 0.0415 cm thick MWCNT-based carbon electrode (1 piece of SGL 10AA) as $Br_2$ electrodes was evaluated in a 1 $cm^2$ $H_2$-$Br_2$ fuel cell. An interdigitated graphite flow field plate was used on the $H_2$ side and a flow-through (1 cm distance between the channels) tantalum plate was used on the $Br_2$ side. The plain SGL 10AA and MWCNT-based carbon electrodes were boiled in DI water and then soaked in 99.9%

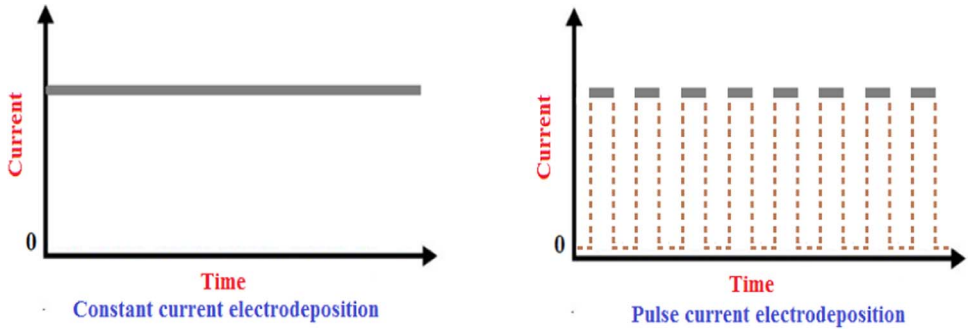


**Figure 3.** Constant and pulse current electrodeposition techniques.

$H_2SO_4$ to improve their wetting characteristics prior to the fuel cell study. A Pt catalyst coated SGL 25BC electrode obtained from TVN systems, Inc. was used as the $H_2$ electrode. The catalyst loading on the hydrogen electrodes was between 0.4 and 0.45 mg-Pt/cm$^2$. The Pt coated SGL 25 BC was hot pressed onto a Nafion 212 membrane (135°C for 5 minutes) and later boiled in DI water for 30 minutes to hydrate the Nafion ionomer present in the membrane electrode assembly (MEA). The MEA and the flow field plates were held in place by two aluminum compression end plates. A mixture of 1 M HBr and 0.9 M $Br_2$ was recirculated through the $Br_2$ electrode at multiple flow rates (10 and 20 cc/min/cm$^2$). Humidified $H_2$ gas at a flow rate of 40 cc/min was pumped through the $H_2$ electrode and vented out at ambient pressure. All the fuel cell experiments were conducted at 25°C unless otherwise specified.

## Results and Discussion

*Constant vs pulse current electrodeposition.*— Figure 3 shows the schematics for constant and pulse current electrodeposition. A constant current for the required amount of time was applied while implementing the constant current electrodeposition technique, whereas the current was applied in short pulses while using pulse current electrodeposition technique. The pulse duration was usually between 0.1 and 10 seconds with a short time gap (1–2 minutes) between the consecutive pulses. The time gap allows the solution concentration near the electrode/electrolyte interface to be replenished. The Co electrodeposition occurs in two steps, nucleation and growth respectively.[30] The nucleation step is where nuclei or seeds are formed on the surface of the carbon fibers which act as sites for the growth of Co nanoparticles. As soon as nuclei were formed, growth occurs simultaneously. At this stage, the nucleation and growth processes are inseparable. The nucleation process stops once the concentration at the carbon electrode/electrolyte interface of the reactant species drops below the minimum concentration (or minimum critical supersaturation level) required for nucleation, and subsequently the growth process is initiated. The size and distribution of Co nanoparticles are determined by both nucleation and growth rates. Depending on the magnitude of the cathodic current applied on the working electrode (WE), the Co catalyst deposition ($Co^{2+} + 2e^- \rightarrow Co$) might occur in either kinetic or mass transport controlled regimes.

While depositing Co catalyst under kinetically controlled regime (low cathodic currents), the nucleation process dominates since the concentration difference of reactant species in the bulk and the carbon electrode/electrolyte interface is negligible. As a result, the electrodeposition of Co proceeds in the formation of layers via nucleation; hence the duration of electrodeposition must be carefully controlled to avoid the formation of a dense layer of Co. On the other hand, the concentration of Co ions at the carbon electrode/electrolyte interface is quickly depleted while electrodepositing Co under mass transport controlled regime. The Co ions from the bulk have to diffuse to the carbon electrode surface to further the electrodeposition. Since the growth process is the dominant mechanism while operating under mass transport controlled regime, there is a high probability of electrodepositing Co nanoparticles.

In this study, the electrodeposition of Co on the first two carbon electrode samples (1 and 2) was done using the constant current technique. As described in the Experimental section, a low current density of −0.1 mA/cm$^2$ was applied to both samples. The small current ensures slow Co electrodeposition rate, providing the best chance to form a dense Co layer. The time spans of electrodeposition for samples 1 and 2 were 1000 s and 2000 s respectively. Figure 4 shows SEM images of samples 1 and 2. As shown in Figure 4, samples 1 and 2 obtained from constant current electrodeposition have a uniform layer of Co on the carbon fiber surface. The Co layer thickens as the span of electrodeposition increases from 1000 (Figure 4a) to 2000 (Figure 4b) seconds. This supports the description given earlier for electrodeposition under kinetically controlled condition.

The remaining samples (3, 4, and 5) were synthesized using pulse current deposition. While conducting pulse current electrodeposition, higher currents with short duration pulses were used. The higher currents applied to the carbon electrode force the Co electrodeposition to occur close to the mass transport controlled regime. Hence, the growth process dominates the electrodeposition mechanisms that lead to Co nanoparticle formation. The deposition current, pulse duration, and number of pulses specified in the Experimental section were used to control the particle size, density, and uniformity. Figure 5 shows the SEM images of samples 3 (−3.75 mA/cm$^2$ for 1s) and 4 (−5 mA/cm$^2$ for 0.2s). The Co nanoparticles with reasonably close packing can be clearly seen in Figure 5. The larger diameter nanoparticles on sample 3 (70 nm–100 nm) in Figure 5a might be a result of longer electrodeposition duration (1s) compared to that of sample 4 (40 nm–60 nm) in Figure 5b (0.2s).

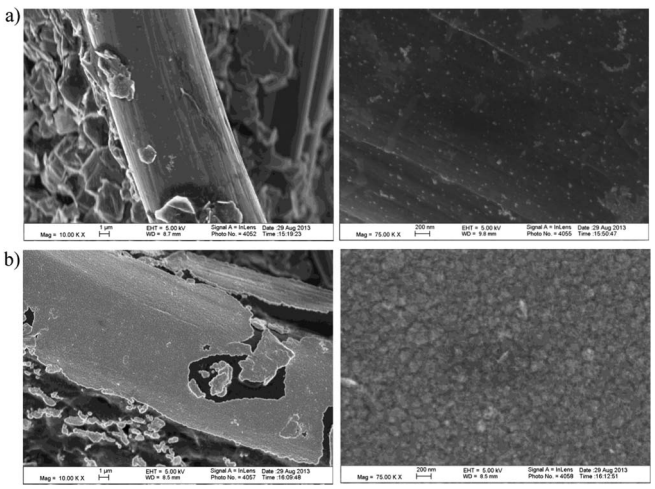


**Figure 4.** Constant current electrodeposition, a) sample 1: −0.1 mA/cm$^2$ for 1000s and b) sample 2: −0.1 mA/cm$^2$ for 2000s.

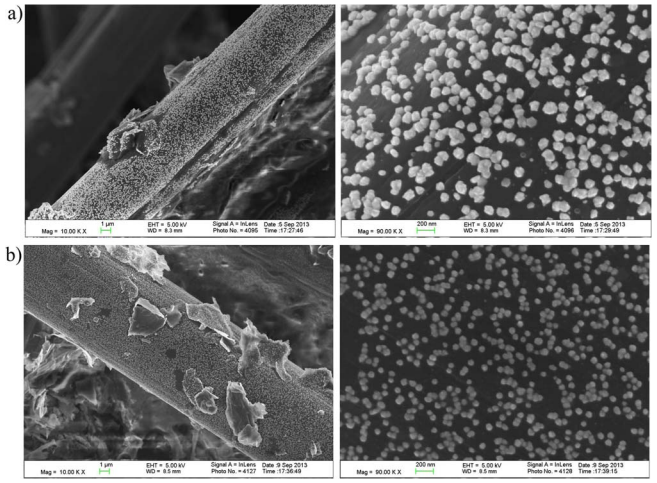

**Figure 5.** Pulse current electrodeposition a) sample 3: $-3.75$ mA/cm$^2$ for 1s and b) sample 4: $-5$ mA/cm$^2$ for 0.2s.

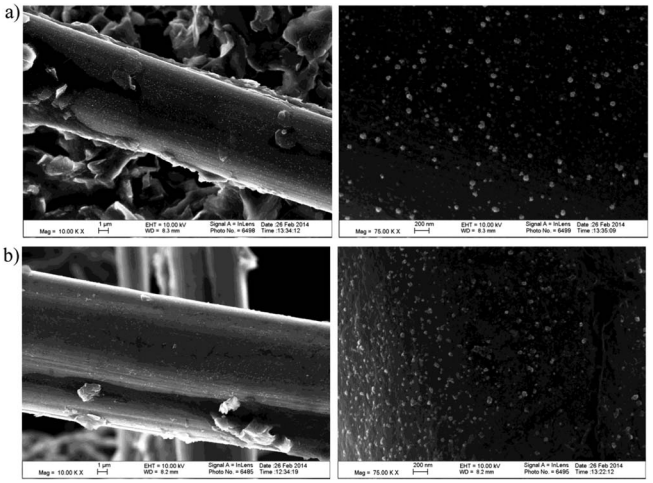

**Figure 6.** Pulse current electrodeposition with the inclusion of presoaking step a) sample 4b (resynthesized): $-5$ mA/cm$^2$ for 0.2s and b) sample 5: $-2.5$ mA/cm$^2$ for 1s.

The next case study was aimed at the effect of pre-soaking carbon electrodes in a precursor solution (mixture of $CoSO_4$ and $H_3BO_3$) prior to the electrodeposition study. The soaking step was included after boiling the samples in DI water and before proceeding to the electrodeposition experiment. The purpose was to enhance the electrodeposition of Co nanoparticles inside the carbon electrode by saturating it with the precursor solution. Sample 4 was synthesized again (labelled as sample 4b) but with the addition of the presoaking step listed above (SEM image shown in Figure 6a). The pre-soaking step assisted in saturating a large section of the electrode surface area of sample 4b with $CoSO_4$, thereby improving the uniformity and the extent of Co electrodeposition. As a result, Co nanoparticles with smaller diameters were electrodeposited throughout the bulk volume of the sample 4b (Figure 6a). Figure 6b shows the SEM image of sample 5 ($-2.5$ mA/cm$^2$ was applied for 1s) that had a presoaking step included. The total charge densities used to synthesize samples 4b and 5 were 1 mC/cm$^2$ and 2.5 mC/cm$^2$ respectively. As shown in Figure 6, the density of Co nanoparticle distribution in sample 5 (Figure 6b) is higher compared to that of sample 4b (Figure 6a). This can be attributed to the higher charge density used to synthesize sample 5. The carbon electrodes with a dense distribution of small Co nanoparticles (Sample 5) were expected to be the ideal candidates for MWCNT growth. Also, the effect of the presoaking step will be discussed further in the Electrochemical analysis section. In conclusion, pulse current electrodeposition appears to be an optimal choice to promote dense distribution of Co nanoparticles.

*MWCNT growth via CVD process.*— The carbon electrodes with electrodeposited Co (samples 1 to 5) were then placed in a quartz tube furnace to facilitate MWCNT growth using the CVD processed described in the Experimental section. The CNT growth proceeded according to two different growth models. Figure 7 shows the tip and base models associated with the CNT growth.[31] According to the tip model, the hydrocarbon gas reacts at the Co nanoparticle/carbon substrate interface and lifts the Co particle as the CNT grows. In this model, the CNT is covalently bonded to the carbon fiber matrix. On the other hand, the CNT grows on top of the nanoparticle according to the base model. The major disadvantage associated with the CNTs grown in accordance with the base model is that the nanotubes are lost once the electrodes are exposed to a corrosive acid environment

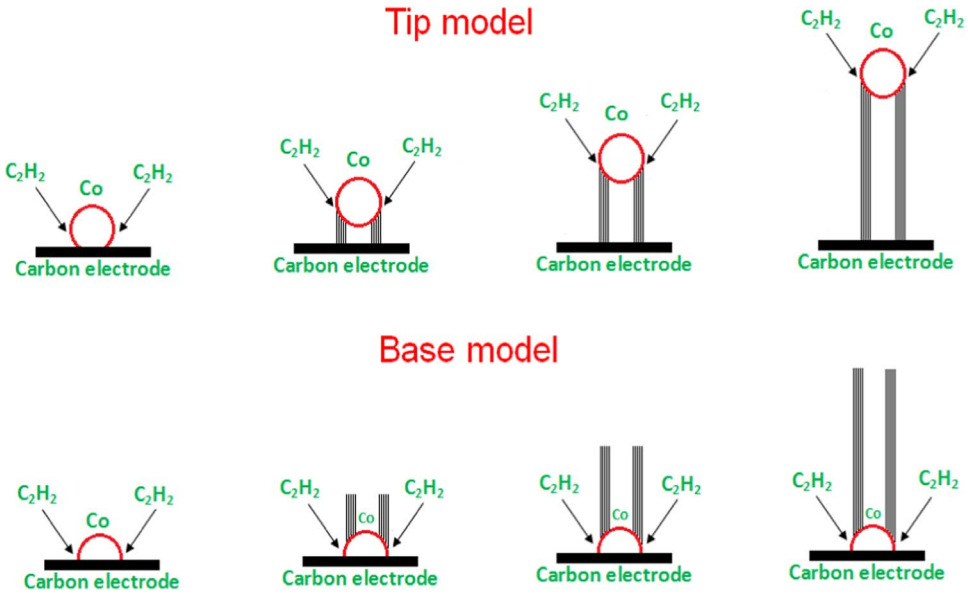


**Figure 7.** Tip and base models explaining the mechanism of MWCNT growth.

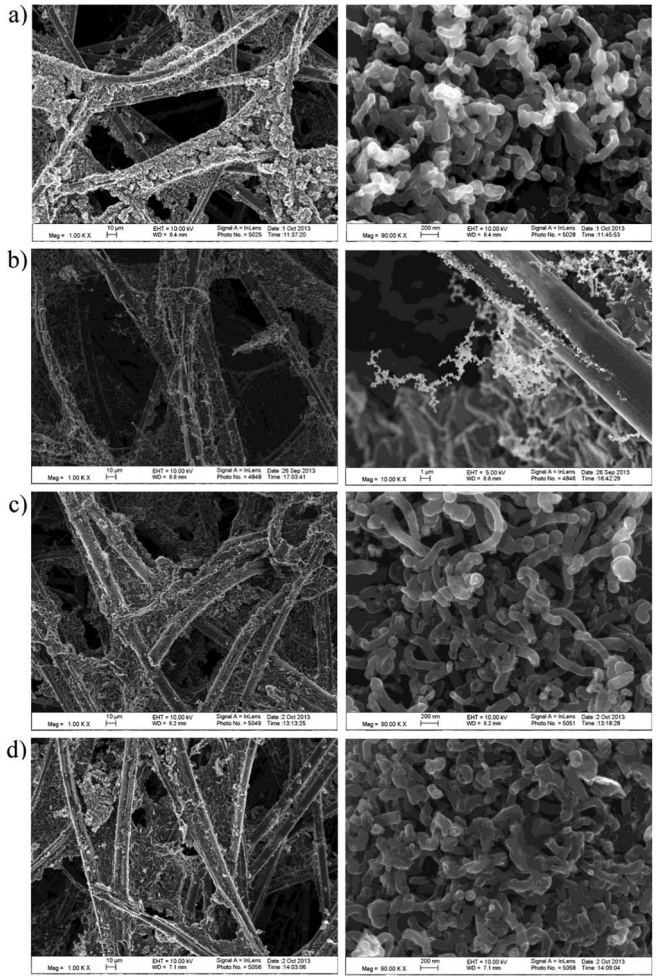


**Figure 8.** Carbon electrodes after MWCNT growth a) sample 1, b) sample 2, c) sample 3, and d) sample 4.

as in the $H_2$-$Br_2$ fuel cell application. The acid etched away the metal nanoparticle connecting the CNT to the carbon electrode fiber surface resulting in the loss of CNTs. Therefore, the tip model is the preferred growth mechanism, because the nanotubes are directly bonded to the carbon electrode.

The SEM images of MWCNT-based carbon electrodes after DI water sonication and acid treatment are shown in Figures 8 and 9. As shown in Figures 8 and 9, the carbon nanotubes remain on all the carbon electrodes, except for sample 2 (Figure 8b), which indicates that the dominant growth mechanism is based on the tip model. The Co layer on sample 2 ($-0.1$ mA/cm$^2$ for 2000s) might be thick enough for the MWCNTs to grow according to the base model, instead of the preferred tip model.[31] As a result, the MWCNTs became separated when the Co nanoparticles underneath them were etched away during the acid pretreatment. On the other hand, the bulk nanotube growth on sample 1 (Figure 8a) could be attributed to its high Co loading compared to rest of the samples. The inset images of Figures 8 and 9 at high resolution show the nanotube growth on the carbon electrode. The diameter of the MWCNTs grown on these samples was between 50 and 70 nm.

The effect of presoaking the electrodes in a mixture of $CoSO_4$ and $H_3BO_3$ prior to electrodeposition on the uniformity MWCNT growth can be clearly seen by comparing Figures 8 and 9. The MWCNT growth on the carbon fibers is more uniform and denser in the pre-soaked electrodes (Figure 9), which can be attributed to the more uniform Co electrodeposition. In order to confirm the growth mechanism of MWCNTs, TEM analysis was conducted. Figure 10 shows the

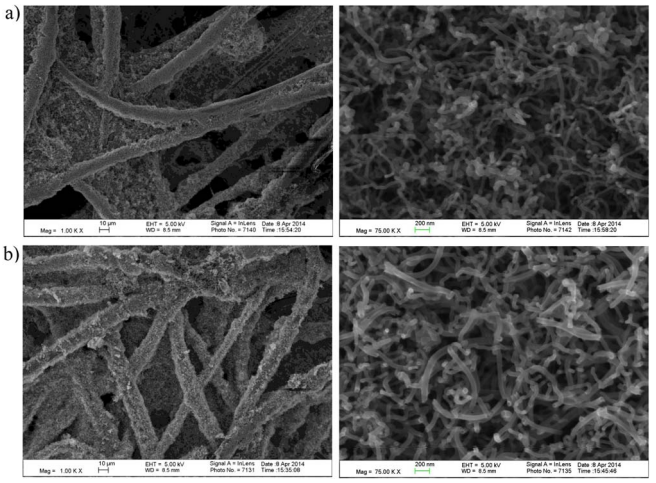


**Figure 9.** Pre-soaked carbon electrodes (in $CoSO_4$ and $H_3BO_3$) after MWCNT growth a) sample 4 (resynthesized) and b) sample 5.

TEM images of the nanotubes grown on these samples. The Co particles trapped inside the MWCNTs were shown in Figure 10a. Also, Figures 10b and 10c clearly show the multiple walls of the carbon nanotube. Finally, the EDX analysis confirmed that the Co nanoparticle is situated at the tip of the nanotube as shown in Figure 10d. The MWCNTs would have a longer life time when the Co nanoparticles were located either at the tip or trapped inside them. Even though Co nanoparticles exposed to the acid environment will be etched away eventually, the covalent bond between MWCNTs and the carbon electrode fiber remains secure due to their growth based on the tip model.

Finally, SEM analysis was done on the carbon electrode regions next to the stainless steel alligator clips (Figure 11a) and the regions 2 cm away (Figure 11b) from them after the electrodeposition process. The aim of this study was to determine the efficiency of stainless steel alligator clips as current collectors. As shown in Figure 11, the limitation associated with using stainless steel alligator clips as current collectors was the non-uniform MWCNT growth on the carbon electrode fiber surface located far from them (seen in the marked portion of Figure 11b). The electronic conductivity of the carbon

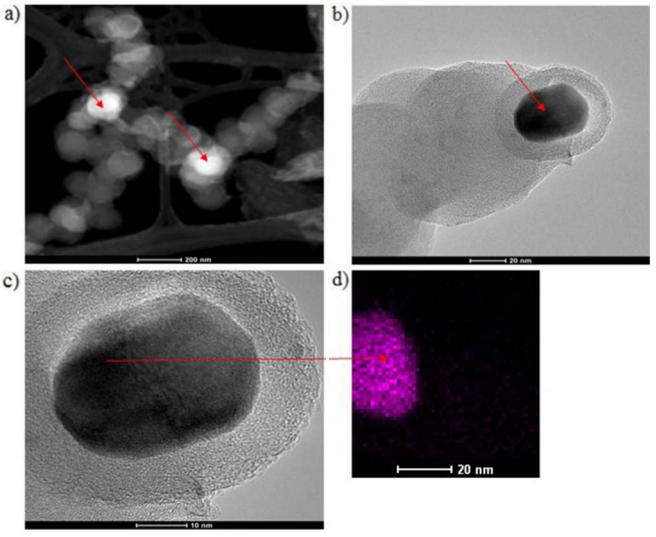


**Figure 10.** TEM images to identify the mechanism of MWCNT growth a) STEM image showing Co nanoparticles trapped inside the MWCNTs, b) TEM image showing a MWCNT, c) TEM image showing multi-walls of the CNT, and d) EDX analysis confirming the Co nanoparticle at the tip of the MWCNT.

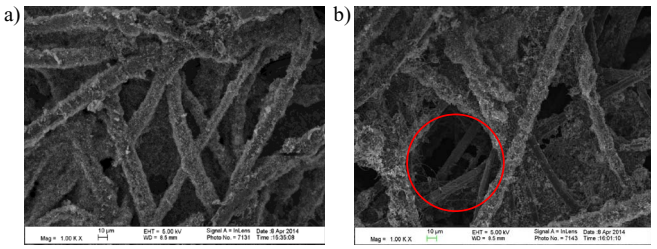


**Figure 11.** SEM images showing the limitation of using alligator clips as current collectors a) SEM image of the carbon electrode region close to the alligator clip and b) SEM image of the carbon electrode region 2 cm from the tip of the alligator clip.

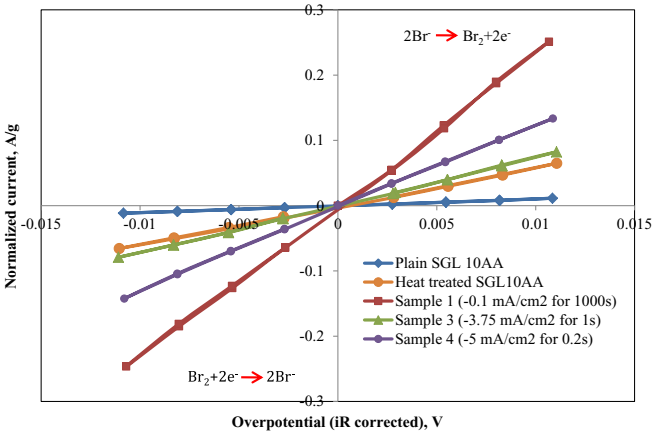


**Figure 12.** Electrochemical analysis of MWCNT-based electrodes in a three-electrode arrangement (heat-treated SGL 10AA, and samples 1, 3, and 4).

electrode was not high enough for the stainless steel alligator clips to promote the electrodeposition of Co nanoparticles and the MWCNT growth over the entire carbon electrode surface area. This effect might be more pronounced when carbon electrodes with large geometric area were used. Currently, efforts are being undertaken to develop current collectors that aid in uniform MWCNT growth over the entire carbon electrode fiber surface area and will be published in a future paper.

*Electrochemical analysis.*— The enhancement factors of the MWCNT-based carbon electrodes were calculated using a three-electrode arrangement as described in the Experimental section. Figures 12 and 13 show the multi-step chronoamperometry plot of plain

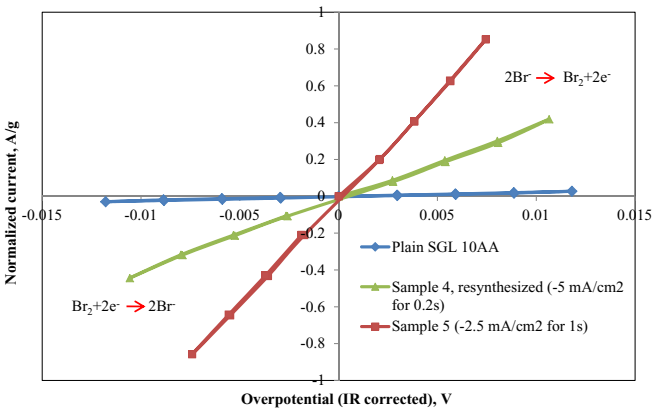


**Figure 13.** Electrochemical analysis of MWCNT-based carbon electrodes (pre-soaked in $CoSO_4$ and $H_3BO_3$ prior to electrodeposition) in a three-electrode arrangement (resynthesized sample 4b and sample 5).

**Table I. Enhancement factor measurements**

| Specimen | Enhancement factor |
|---|---|
| Heat-treated SGL 10AA | 5 |
| Sample 1 | 22 |
| Sample 3 | 7 |
| Sample 4 | 11 |
| Sample 4b (resynthesized) | 17 |
| Sample 5 | 50 |

SGL 10AA, heat-treated SGL 10AA, and MWCNT-based carbon electrodes. The overpotentials in Figures 12 and 13 were corrected for ohmic loss using the resistance measured by EIS. The product of the active surface area ($a$) and exchange current density ($i_o$) was calculated from the slope ($\frac{di}{d\eta}$) of the multi-step chronoamperometry plot. The factor $ai_o$ for all the electrodes are normalized to the value of a plain SGL 10AA carbon electrode to calculate the enhancement factors (Equation 2). Even though the exchange current density of a carbon GDE substrate might be different from that of MWCNTs, it is the product of active area and exchange current density that contributes to the effective activity enhancement. As show in Table I, enhancement factors between 7 and 50 were achieved by using the MWCNT-based carbon electrodes (samples 1, 3, 4, and 5). The active surface area of the heat-treated carbon electrode was found be 5 times higher than that of a plain carbon electrode. However, the active surface area enhancement factor of the heat-treated carbon electrode was lower than those of the MWCNT-based carbon electrodes. The enhancement factor of sample 4 ($-5$ mA/cm$^2$ for 0.2 s) was improved (enhancement factor from 11 to 17) upon presoaking it in $CoSO_4$ and $H_3BO_3$ solution prior to electrodeposition. This might be a result of uniform Co nanoparticle deposition over a large carbon fiber surface area on the pre-soaked sample. Also, an enhancement factor of 50 was achieved with sample 5 ($-2.5$ mA/cm$^2$ for 1s). The smaller nanoparticle size with dense distribution observed in the SEM images of sample 5 has contributed to the significant active area enhancement.

*Fuel cell measurements.*— Finally, the performance of the MWCNT-based carbon electrode (sample 5) was measured in a $H_2$-$Br_2$ fuel cell. As shown in Figure 14, the discharge performance of a single layer of MWCNT electrode is almost equal or slightly higher when compared to that of the 3-layer plain SGL 10 AA electrode at lower flow rate (10 cc/min/cm$^2$ used for MWCNT electrode vs 20 cc/min/cm$^2$ used for 3 piece SGL 10AA). A single layer of MWCNT electrode not only provided more active surface

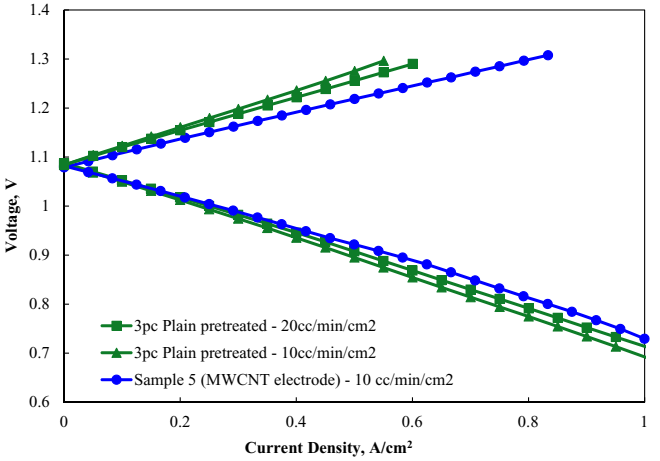


**Figure 14.** Performance comparison between 3 layers of plain SGL 10AA and sample 5 (MWCNT electrode) in an actual $H_2$-$Br_2$ fuel cell.

area for the bromine reactions but also reduced the mass-transport distance since its thickness was only one-third that of the 3-layer plain SGL 10AA electrode. The performance of the MWCNT electrode was very promising in terms of offering better performance and cost benefits. Both the bromine electrode and pumping costs might be reduced by employing a MWCNT electrode instead of using multiple layers of a plain carbon electrode. Currently, the electrodeposition and CVD processes are being optimized to enhance the performance of the MWCNT-based carbon electrodes.

## Conclusions

The widely used commercial plain carbon electrodes for $Br_2$ reactions usually have low specific surface areas. In this paper, a study regarding the growth of MWCNTs directly on the carbon electrode fiber surface to improve the active surface area of conventionally used plain SGL 10AA carbon electrodes was discussed. The Co catalyst was electrodeposited using both constant and pulse current electrodeposition techniques. Subsequently, the Co catalyzed MWCNT growth was accomplished using the CVD process. The presoaking of carbon electrodes in a mixture of $CoSO_4$ and $H_3BO_3$ prior to electrodeposition led to more uniform Co nanoparticle deposition and MWCNT growth over a larger portion of the carbon electrode fiber surface. Active area enhancement factors between 7 and 50 were achieved using MWCNT-based carbon electrodes. Finally, the performance of MWCNT-based carbon electrode (enhancement factor of 50) in a $H_2$-$Br_2$ fuel cell was found to be equal or slightly better compared to that of a plain SGL 10AA (3 layers) carbon electrode. In conclusion, the performance of MWCNT electrodes looks promising and might play a role in reducing the bromine electrode and pumping costs.

## Acknowledgments

The authors acknowledge the financial support of this work by the National Science Foundation through grant no. EFRI-1038234 and ARPA-E program under Department of Energy through grant number AR0000262.

## References

1. T. Nguyen and R. Savinell, *Electrochemical Society Interface*, **19**(3), 54 (2010).
2. W. Glass and G. H. Boyle, *Advances in Chemistry Series*, **47**, 203 (1965).
3. R. S. Yeo and D. T. Chin, *J. Electrochem. Soc.*, **127**(3), 549 (1980).
4. G. G. Barna, S. N. Frank, T. H. Teherani, and L. D. Weedon, *J. Electrochem. Soc.*, **131**(9), 1973 (1984).
5. V. Livshits, A. Ulus, and E. Peled, *Electrochemistry Communications*, **8**, 1358 (2006).
6. K. T. Cho, P. Ridgeway, Adam Z. Weber, S. Haussener, V. Battagalia, and V. Srinivasan, *J. Electrochem. Soc.*, **159**(11), A1806 (2012).
7. H. Kreutzer, V. Yarlagadda, and T. V. Nguyen, *J. Electrochem Soc*., **159**(7), F331 (2012).
8. Michael C. Tucker, K. T. Cho, Adam Z. Weber, G. Lin, and T. V. Nguyen, *J. Appl. Electrochem.*, **45**, 11 (2015).
9. V. Yufit, B. Hale, M. Matian, P. Mazur, and N. P. Brandon, *J. Electrochem Soc.*, **160**(6), A856 (2013).
10. M. Goor-Dar, N. Travitsky, and E. Peled, *J. Power Sources*, **197**, 111 (2012).
11. C.-N. Sun, F. M. Delnick, D. S. Aaron, A. B. Papandrew, M. M. Mench, and T. A. Zawodzinski, *ECS Electrochemistry Letters*, **2**(5), A43 (2013).
12. V. Yarlagadda and T. V. Nguyen, *J. Electrochem Soc*., **160**(6), F535 (2013).
13. S. Stankovich, Dmitriy A. Dikin, Richard D. Piner, Kevin A. Kohlhaas, A. Kleinhammes, Y. Jia, Y. Wu, SonhBinh T. Nguyen, and Rodney S. Ruoff, *Carbon*, **45**, 1558 (2007).
14. Y. Zhai, Y. Dou, D. Zhao, Pasquale F. Fulvio, Richard T. Mayes, and S. Dai, *Adv. Mater.*, **23**, 4828 (2011).
15. D. Tashima, A. Sakamoto, M. Taniguchi, T. Sakoda, and M. Otsubo, *Vacuum*, **83**, 695 (2009).
16. C. Ma, Y. Li, J. Shi, Y. Song, and L. Liu, *Chemical Engineering Journal*, **249**, 216 (2014).
17. I. Mayrhuber, C. R. Dennison, V. Kalra, and E. C. Kumbur, *J. Power Sources*, **260**, 251 (2014).
18. C. Wang, M. Waje, X. Wang, J. M. Tang, R. C. Haddon, and Y. Yan, *Nano Letters*, **4**(2), 345 (2004).
19. C. Du, B. Wang, and X. Cheng, *J. Power Sources*, **187**, 505 (2009).
20. B. Kim, H. Chung, and W. Kim, *J. Phys. Chem. C.*, **114**, 15223 (2010).
21. C.-T. Hsieh, H. Teng, W.-Y. Chen, and Y.-S. Cheng, *Carbon*, **48**, 4219 (2010).
22. J. Prasek, J. Drbohlavova, J. Chomoucka, J. Hubalek, O. Jasek, V. Adam, and R. Kizek, *J. Mater. Chem.*, **21**, 15872 (2011).
23. N. Sinha and John T.-W. Yeow, *IEEE Transactions on Nanobioscience*, **4**(2), 180 (2005).
24. H. Dai, *Acc. Chem. Res.*, **35**, 1035 (2002).
25. S. Ijima, *Nature*, **354**, 56 (1991).
26. J.-P. Tessonnier and D. S. Su, *ChemSusChem*, **4**(7), 824 (2011).
27. Z. Yang, X. Chen, H. Nie, K. Zhang, W. Li, B. Yi, and L. Xu, *Nanotechnology*, **19**, 1 (2008).
28. Q. Zhang, J. Lu, R. Sager, L. Dai, and J. Baur, *J. Compscitech*, **69**, 594 (2009).
29. J. Vanpaemel, M. H. Van Der Veen, C. Huyghebaert, S. De Gendt, and P. M. Vereecken, *ECS Transactions*, **50**(20), 29 (2013).
30. Nguyen T. K. Thanh, N. Maclean, and S. Mahiddine, *J. Chem. Rev.*, **114**, 7610 (2014).
31. M. Kumar and Y. Ando, *J. Nanosci. Nanotechnol.*, **10**, 3739 (2010).